Multi-Harmonic Nonlinear Modeling of Low-power PWM DC-DC Converters operating in CCM and DCM

Ya Wang
Department of Electrical and
Computer Engineering
Texas A&M University
College Station, TX 77843
tonywang@tamu.edu

Di Gao
Department of Electrical and
Computer Engineering
Texas A&M University
College Station, TX 77843
gaodi0928@tamu.edu

Dani A. Tannir
Department of Electrical and
Computer Engineering
Lebanese American University
P.O. Box 36, Byblos, Lebanon
dani.tannir@lau.edu.lb

Peng Li
Department of Electrical and
Computer Engineering
Texas A&M University
College Station, TX 77843
pli@tamu.edu

Abstract—**DC-DC converters form an essential component of modern low-power integrated circuits. This paper presents a novel nonlinear modeling technique for pulse-width modulated (PWM) DC-DC converters for low-power applications. Our enhanced model not only predicts the dc response, but also captures harmonics of arbitrary degrees. The proposed full-order model retains the inductor current as a state variable and accurately captures the circuit dynamics even in the transient state. Furthermore, by continuously monitoring state variables, our model seamlessly transitions between continuous conduction mode (CCM) and discontinuous conduction mode (DCM), which often occurs in low-power applications while also accounting for the non-idealities of the circuit devices. The proposed model, when tested with a system decoupling technique, obtains up to $10X$ runtime speedups over transistor-level simulations with a maximum output voltage error that never exceeds 4%.**

I. Introduction

The transient simulation of power management circuits such as DC-DC converters is generally very time-consuming due to the co-existence of fast switching activities and slow load variations. Circuit averaging techniques are well suited for the efficient simulation of DC-DC converters. In particular, state-space averaging has been a very popular simulation technique of pulse-width modulated (PWM) DC-DC converters. In [1], [2], [3], both large-signal and small-signal state-space average models for DC-DC converters operating in continuous conduction mode (CCM) and Discontinuous Conduction Mode (DCM) are presented. However, without considering non-ideal device characteristics, [2] and [3] are inaccurate in simulating low-power DC-DC converters. Furthermore, the modeling approach of [2] and [3] is circuit-specific, thereby limiting the ability to automate the modeling and simulation process on arbitrary DC-DC converter topologies.

Alternatively, the PWM switch model [4][5], which is a linearization of the three-terminal switch cell, can be readily applied to a wide range of DC-DC converters. By tracking the circuit operating mode based on averaged circuit states, [6] enhances the basic PWM switch model to support simulation of DC-DC converters operating in both CCM and DCM. However, a major limitation of the PWM switch model is that it neglects the dynamic behavior of DC-DC converters within one cycle and provides no information about the waveform ripples. As suggested in [7], the PWM switch model has an underlying assumption of the small ripple condition, which prevents it from being applied to converters with large ripples.

It has been shown that neglecting the ripples of state variables can lead to large discrepancies in the simulation results of converters operating at low frequencies [8].

To address this problem, a lot of work has been done on the generalized averaging techniques [9]. In [8], a multi-frequency averaged model is introduced which conducts frequency selective averaging on the switched state-space models of DC-DC converters. However, this method is based on boost converters and cannot be easily applied to other converter configurations. In [10], a flexible method of in-place averaging that replaces elements in DC-DC converters with the kth-index average elements is presented, thereby allowing for the tracking of responses with harmonics up to k^{th} degree. However, the method in [10] assumes a continuous inductor current with ideal switches. As a result, such a model becomes neither suitable nor accurate enough for low-power DC-DC converter simulations.

In this paper, we present a complete solution to low-power PWM DC-DC converter simulations. The proposed solution combines the accuracy of enhanced state-space averaging, the flexibility of PWM switch models and the multi-frequency nature of the generalized models. The proposed model has four main features. First, the model approximates the actual converter responses by multiple harmonics of ripples up to an arbitrary degree. Second, the model accounts for the effects of device non-idealities like diode forward voltage drop in an efficient manner. The third feature lies in its generality. Our proposed model is based on the switch cell and can be applied to many DC-DC converters including buck, boost and buck-boost converters without any modifications. It is also general in the sense that both CCM and DCM operations are supported. Finally, a system decoupling technique is introduced to simulate converters with improved efficiency. As a result, when applied to several open-loop DC-DC converters, the proposed model generates almost identical responses as the transistor-level simulations with a runtime speedup of one order of magnitude.

II. Generalized Switch Model with Device Non-idealities

In this section, we present a generalized model of a three-terminal switch cell based on a standard buck converter shown in Fig. 1(a). The generalized switch model can also be applied to other PWM DC-DC converters with no additional changes.
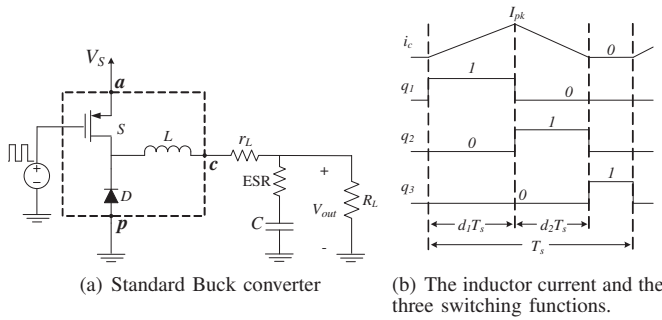
(a) Standard Buck converter   (b) The inductor current and the three switching functions.

Fig. 1. Standard Buck PWM DC-DC converter

Fig. 3. The equivalent model of the switch cell with non-ideal device characteristics.

To accurately capture the circuit behavior, the dynamic non-idealities are accounted for in the switch cell. Furthermore, by continuously monitoring the circuit state, our model seamlessly transitions between CCM and DCM.

A. Equivalent switch model based on switching functions

Consider the buck converter shown in Fig. 1(a) operating in DCM with a discontinuous inductor current i_c shown in Fig. 1(b). The switching cycle T_s is divided into three operation intervals by three binary switching functions $q_1(t)$, $q_2(t)$ and $q_3(t)$ using the parameters d_1 and d_2 as shown in Fig. 1(b). Fig. 2 (a) shows the extracted switch cell while Figs. 2 (b),(c) and (d) show the three equivalent circuits corresponding to the three intervals.

Next, we analyze two circuit variables, v_{ag} and i_p, of particular interest in each operation interval and construct a complete nonlinear DCM switch model. In the first interval, the MOS transistor operates in the triode region with a nonlinear resistance of $R_{ds(on)}$ resulting in a voltage drop of $V_{ds(on)}$ while the diode is reverse biased. As shown in Fig. 2(b), in the first interval, we have $v_{ag} = q_1 V_{ds(on)}$ and $i_p = 0$. In the second interval, the diode is forward biased and holds a forward voltage drop V_d while the MOS transistor is operating in sub-threshold conduction with a leakage current I_{leak}. An equivalent resistor $R_{ds(off)}$ is used to model the effect of sub-threshold conduction. As shown in Fig. 2(c), in the second interval we have $v_{ag} = q_2 (v_{ap} + V_d)$ and $i_p = q_2 (i_c - I_{leak})$.
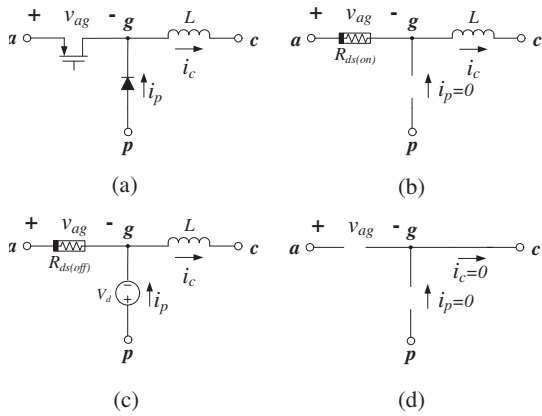
In the third interval, the inductor is completely discharged and the inductor current is zero. Both the transistor and the diode are off. According to the constitutive equation of inductors $v_L(t) = L\frac{di_L(t)}{dt}$, the inductor is shortened such that $v_{gc} = 0$. In the third interval, we have $V_{ag} = q_3 V_{ac}$ and $i_p = 0$. Combining the expressions of V_{ag} and i_p over the three intervals results in:

$$v_{ag} = q_1(t)V_{ds(on)} + q_2(t)(v_{ap} + V_d) + q_3(t)v_{ac} \quad (1)$$
$$i_p = q_2(t)(i_c - I_{leak}). \quad (2)$$

We can now replace the transistor and the diode in the original circuit by controlled sources using the relations in (1) and in (2). This leads to the model shown in Fig. 3, which is essentially an equivalent switch model that accounts for the non-ideal device characteristics. Inserting the model of Fig. 3 in place of the switch cell in Fig. 1(a) results in a circuit model that accurately captures the behavior of the converter.

The switch model can also be applied to converters operating in CCM with one additional constraint of $d_1 + d_2 = 1$. The process of determining the operation mode is automated by calculating d_2 concurrently as the model is being simulated using

$$d_2 = \frac{2L}{d_1 T_s}\frac{\bar{i}_c}{\bar{v}_{ac} - V_{ds(on)}} - d_1, \quad (3)$$

where $\bar{i}_c$ and $\bar{v}_{ac}$ are the average inductor current and the average voltage across nodes a and c in one cycle, both of which are immediately available in the multi-harmonic model as will be shown later. If $d_1 + d_2 < 1$, the converter operates in DCM. Otherwise, it operates in CCM with $d_2 = 1 - d_1$[5]. Note that(3) accounts for the non-idealities of the transistors and therefore results into a more accurate evaluation of d_2 than [3].

B. Non-ideal device modeling and the complete equivalent converter model

The accuracy of the model in Fig. 3 depends on the evaluation of $V_{ds(on)}$, V_d and I_{leak}, which are nonlinear functions of the circuit state and vary dynamically during the circuit simulation. These three values can be evaluated without simulating the actual buck converter, but by exploiting the information available in the equivalent model in Fig. 3. The process is illustrated by the example of computing $V_{ds(on)}$ shown in Fig. 4, where a buck converter is operating in the first interval with transistor Q_1 in the triode region with a limited conductance between the drain and the source. Due to the presence of a nonlinear resistance $R_{ds(on)}$, a voltage drop of $V_{ds(on)}$ is found between the drain and the source.

Fig. 2. The three-terminal switch cell(a) and its equivalent circuits in three operation intervals (b)(c)(d).

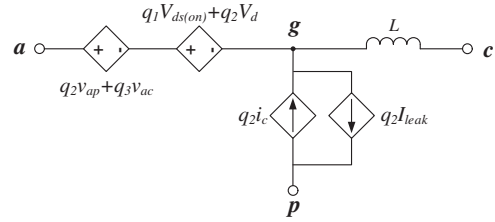*2016 Design, Automation & Test in Europe Conference & Exhibition (DATE)*
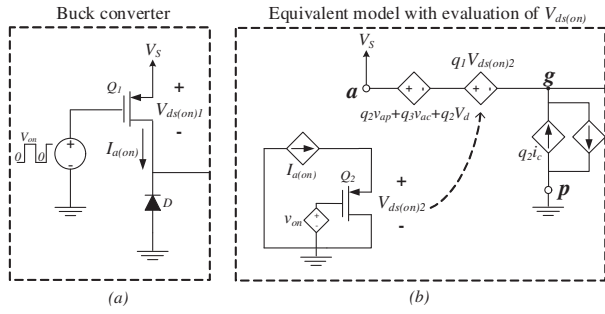
Fig. 4. A buck converter operating at the first interval(a) and its equivalent model with an additional circuit to evaluate the voltage drop $V_{ds(on)}$ using an accurate device model(b).

In the equivalent model, the evaluation of the voltage drop $V_{ds(on)}$ is achieved by adding the additional circuit shown in Fig. 4(b), which is constructed such that transistor Q_2 has the same bias (i.e. gate-to-source voltage and drain-to-source current) as transistor Q_1. To achieve this, we observe that in the first interval the drain-to-source current of Q_1 corresponds to $I_{a(on)}$ of the equivalent model and the gate-to-source voltage of Q_1 is V_{on}. Thus by forcing the drain-to-source current of Q_2 to be $I_{a(on)}$ and connecting the gate of Q_2 to the voltage source V_{on}, we ensure that the voltage drop produced by Q_2 is the same as that of Q_1 in the buck converter. Returning the voltage drop of Q_2 to the equivalent model allows the model to account for this type of non-ideality. It is important to note that the transistor Q_2 uses the same device model as Q_1(e.g. BSIM3/4). Thus the behaviour captured by transistor Q_2 fully accounts for the device non-idealities of Q_1.

Similar procedures can be used to obtain I_{leak} and V_d. With three additional circuits included, the complete equivalent model automatically accounts for all non-ideal device characteristics. By including simple additional transistor circuits as shown in Fig. 4(b), we are able to construct a coupled DC-DC converter model in which essential device non-idealities from the MOS switch and the diode can be accurately evaluated as part of the overall converter model.

III. EFFICIENT MULTI-HARMONIC MODELING OF THE SWITCH CELL

Fig. 3 presents a switch model with non-ideal device characteristics. However, it is essentially a switching circuit due to the presence of $q(t)$ and is computationally expensive for performing transient simulations. In this section, we propose a multi-harmonic averaged model that is both accurate and efficient. The proposed model approximates the true response of a DC-DC converter using a Fourier series of any order of choice. Since the switching functions $q(t)$ are decomposed into several Fourier series and are no longer present in the model, the proposed model is highly efficient.

A. Multi-harmonic model of switch cell

Multi-harmonic modeling decomposes each state variable into a Fourier series. Recall that a time-domain periodic signal $x(\tau)$ can be expanded using the Fourier series as

$$x(\tau) = \sum_{k=-\infty}^{\infty} \langle x \rangle_k(t) e^{jk\omega_s \tau}, \qquad (4)$$

where $\omega_s = 2\pi f_s$ and f_s is the switching frequency. $\langle x \rangle_k(t)$ is the kth complex Fourier coefficient[7], which is given by

$$\langle x \rangle_k(t) = \frac{1}{T_s} \int_{t-T_s}^{t} x(\tau) e^{-jk\omega_s \tau} d\tau. \qquad (5)$$

As shown in (5), $\langle x \rangle_k(t)$ is defined by taking the average of $x(\tau)$ at a frequency kf_s. For instance, $\langle x \rangle_0(t)$ represents the dc component and $\langle x \rangle_1(t)$ represents the harmonic component at the fundamental frequency. Thus, we denote $\langle x \rangle_k(t)$ by the index-k average. By including higher orders of harmonics, the multi-harmonic model is able to approximate the non-linear behaviour of the switch cell with higher accuracy. However, as a result, the multi-harmonic model becomes more complex in circuit topology and more time-consuming to solve. Essentially a trade off needs to be found between the accuracy and efficiency of the multi-harmonic model. In [11], the FFT analysis of a typical DC-DC converter indicates that the voltage response is mainly composed of the dc and the first order harmonic. For these reasons, we will only the index-0 and the index-1 averages in the multi-harmonic model.

According to [8], two properties can be immediately identified from (4) and (5) that allow us to calculate the index-k averages of the switch model. The first property is discrete convolution. Using this property, each index-0 average term in (1) and (2) can be written as

$$\langle qx \rangle_k = \langle q \rangle_0 \langle x \rangle_0 + \langle q \rangle_1 \langle x \rangle_{-1} + \langle q \rangle_{-1} \langle x \rangle_1. \qquad (6)$$

According to (5), every complex Fourier coefficient includes a real and an imaginary part. We also know that $\langle x \rangle_k$ and $\langle x \rangle_{-k}$ are conjugates of each other, which means $\langle x \rangle_k^R = \langle x \rangle_{-k}^R$ and $\langle x \rangle_k^I = -\langle x \rangle_{-k}^I$. Exploiting the conjugation property provides the following expression for the index-0 average of a product

$$\langle qx \rangle_0 = \langle q \rangle_0 \langle x \rangle_0 + 2 \left(\langle q \rangle_1^R \langle x \rangle_1^R + \langle q \rangle_1^I \langle x \rangle_1^I \right). \qquad (7)$$

Substituting (7) into (1) and (2) gives the index-0 average model of the switch cell as follows

$$
\begin{aligned}
\langle v_{ag} \rangle_0 =& \langle q_1 \rangle_0 V_{ds(on)} + \langle q_2 \rangle_0 V_d \\
&+ \langle q_2 \rangle_0 \langle v_{ap} \rangle_0 + 2 \left(\langle q_2 \rangle_1^R \langle v_{ap} \rangle_1^R + \langle q_2 \rangle_1^I \langle v_{ap} \rangle_1^I \right) \\
&+ \langle q_3 \rangle_0 \langle v_{ac} \rangle_0 + 2 \left(\langle q_3 \rangle_1^R \langle v_{ac} \rangle_1^R + \langle q_3 \rangle_1^I \langle v_{ac} \rangle_1^I \right) \quad (8) \\
\langle i_p \rangle_0 =& \langle q_2 \rangle_0 \cdot I_{leak} \\
&+ \langle q_2 \rangle_0 \langle i_c \rangle_0 + 2 \left(\langle q_2 \rangle_1^R \langle i_c \rangle_1^R + \langle q_2 \rangle_1^I \langle i_c \rangle_1^I \right).
\end{aligned}
$$

Similarly, the index-1 average of a product is given by

$$\langle qx \rangle_1^R = \langle q \rangle_0 \langle x \rangle_1^R + \langle q \rangle_1^R \langle x \rangle_0 \qquad (9)$$
$$\langle qx \rangle_1^I = \langle q \rangle_0 \langle x \rangle_1^I + \langle q \rangle_1^I \langle x \rangle_0. \qquad (10)$$

Substituting (9) and (10) into (1) and (2) gives the real part of the index-1 average model of the switch cell as

$$
\begin{aligned}
\langle v_{ag} \rangle_1^R =& \langle q_1 \rangle_1^R V_{ds(on)} + \langle q_2 \rangle_0 \langle v_{ap} \rangle_1^R + \langle q_2 \rangle_1^R \langle v_{ap} \rangle_0 \\
&+ \langle q_2 \rangle_1^R \cdot V_d + \langle q_3 \rangle_0 \langle v_{ac} \rangle_1^R + \langle q_3 \rangle_1^R \langle v_{ac} \rangle_0 \quad (11) \\
\langle i_p \rangle_1^R =& \langle q_2 \rangle_0 \cdot I_{leak} + \langle q_2 \rangle_0 \langle i_c \rangle_1^R + \langle q_2 \rangle_1^R \langle i_c \rangle_0,
\end{aligned}
$$

and the imaginary part of the index-1 average model as

$$
\begin{aligned}
\langle v_{ag} \rangle_1^I =& \langle q_1 \rangle_1^I V_{ds(on)} + \langle q_2 \rangle_0 \langle v_{ap} \rangle_1^I + \langle q_2 \rangle_1^I \langle v_{ap} \rangle_0 \\
&+ \langle q_2 \rangle_1^I \cdot V_d + \langle q_3 \rangle_0 \langle v_{ac} \rangle_1^I + \langle q_3 \rangle_1^I \langle v_{ac} \rangle_0 \quad (12) \\
\langle i_p \rangle_1^I =& \langle q_2 \rangle_0 \cdot I_{leak} + \langle q_2 \rangle_0 \langle i_c \rangle_1^I + \langle q_2 \rangle_1^I \langle i_c \rangle_0.
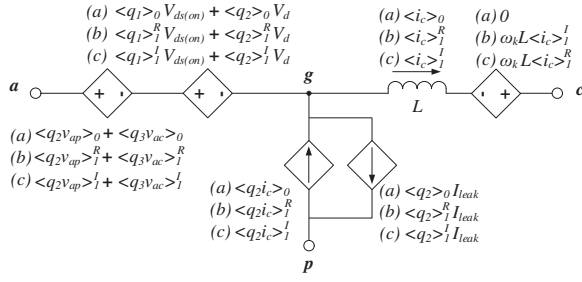\end{aligned}
$$

Fig. 5. The multi-harmonic model of the three-terminal the switch cell including (a) index-0 average model, (b) the real part of index-1 average model and (c) the imaginary part of index-1 average model.
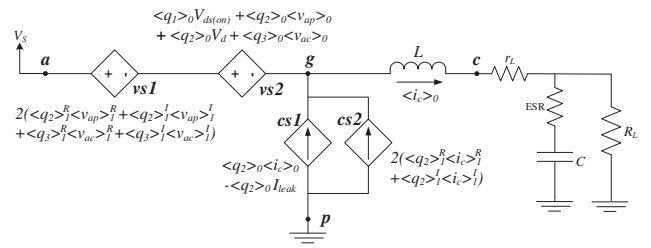

Fig. 6. The index-0 average model of the buck converter. Controlled sources $vs1$ and $cs2$ depend on the index-1 average model and will be completely removed in the decoupled index-0 average model.

The second property we exploit is the average of differentiation

$$\langle \frac{dx}{dt} \rangle_k(t) = \frac{d\langle x \rangle_k(t)}{dt} + jk\omega_s \langle x \rangle_k(t). \quad (13)$$

Applying (13) to the constitutive equation of inductors $v_L = L\frac{di_L}{dt}$ reveals that an index-k average of an inductor can be modeled by an inductor model with the same inductance in series with an impedance of $jk\omega_s L$.

Combining (8), (11), (12) and (13) produces the final model of the switch including index-0 and index-1 averages, as shown in Fig. 5. It should also be noted that a multi-harmonic model is generally highly coupled due to the interactions between averages of different orders.

B. Multi-harmonic model of the DC-DC converter

Apart from the switch cell, we need to find the index-k model for all other components of the DC-DC converter, e.g. the load capacitor and parasitic resistors. By the definition of index-k average shown in (5), it is easy to verify that $\langle v_R \rangle_k = R\langle i_R \rangle_k$, which implies the index-k average of a resistor has the same branch constitutive relationship of the resistor in terms of the branch voltage and current. Like the index-k average of an inductor, a physical capacitor can be modeled as an average capacitor model with the same capacitance in parallel with an admittance of $jk w_s C$.

Using the multi-harmonic average models for the switch cell in addition to the capacitors and the resistors derived above, we construct an index-0 and index-1 average model of a DC-DC converter. This results in three coupled circuits, which can be solved for the dc and the first-order harmonic responses.

IV. SYSTEM DECOUPLING

As pointed out earlier, solving mutually dependent averages of different orders is a computationally intensive task. In this section, we provide two rules for system decoupling that can remove the dependency of 0-index average models on all higher order models, which also improves the model accuracy.

Consider the standard buck converter shown in Fig. 1(a) and its 0-index average model shown in Fig. 6. Our objective is to remove the VCVS $vs1$ and the CCCS $cs2$, both of which depend on components from the index-1 average model. Recall that the index-0 average of a product can be evaluated from the discrete convolution relation by (6). One useful observation is that if x has a very small variance within one cycle and hence

can be viewed as a constant, then for any $k \neq 0$, $\langle x \rangle_k = 0$. Thus, we suggest the first rule of system decoupling:

Rule 1: If x has small variance within one cycle, then $\langle qx \rangle_0 \approx \langle q \rangle_0 \langle x \rangle_0$. All higher order terms can be removed from the index-0 average calculation while only introducing negligible errors.

In Fig. 5(a), there are three averages of product terms $\langle q_2 v_{ap} \rangle_0$, $\langle q_3 v_{ac} \rangle_0$ and $\langle q_2 i_c \rangle_0$. In the buck converter, we have $v_{ap} = V_s$ and $v_{ac} = V_s - V_{out}$, where V_s denotes the supply voltage and V_{out} dc component of the output voltage. Thus the voltage swings in v_{ap} and v_{ac} are small and can be neglected. Therefore, we can apply rule 1 to $\langle q_2 v_{ap} \rangle_0$ and $\langle q_3 v_{ac} \rangle_0$ for the case of buck converters. This results in the complete removal of $vs1$ in Fig. 6.

On the other hand, $\langle q_2 i_c \rangle_0$ cannot be simplified by rule 1 due to the large variance of i_c shown in Fig. 7(a). (7) computeds the discrete convolution of $\langle q_2 i_c \rangle_0$, which includes the index-1 terms. To remove these terms, we need to consider the shape of i_c and q_2. In Fig. 7(a), the index-0 average value of i_c is essentially the dc value of the inductor current, which can be calculated by dividing the shaded area by the total time interval

$$\langle i_c \rangle_0 = \bar{i}_c = \frac{1}{2}(d_1 + d_2)I_{pk}, \quad (14)$$

where $d_1 = \langle q_1 \rangle_0$, $d_2 = \langle q_2 \rangle_0$ and I_{pk} is the peak value of i_c. Similarly, the index-0 average value of $q_2 i_c$ is

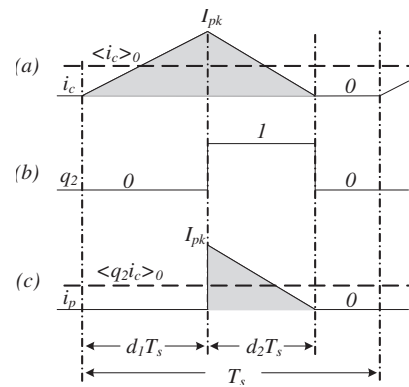$$\langle q_2 i_c \rangle_0 = \bar{i}_p = \frac{1}{2}d_2 I_{pk}. \quad (15)$$

Fig. 7. Illustration of $\langle q_2 i_c \rangle_0$ calculation: (a) inductor current i_c, (b) switch function q_2, and (c) product term $q_2 i_c$. The 0-index average can be calculated by dividing the shaded area by the length of interval.
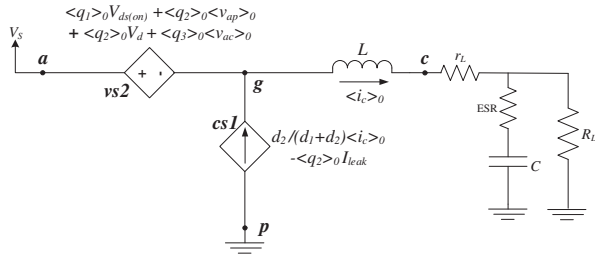
Fig. 8. The decoupled index-0 average model of the buck converter.

Fig. 9. A standard boost converter with $V_s = 2V$, $L = 300\mu H$, $C = 1\mu F$ and $R_L = 50\Omega$.

Substituting (14) into (15) leads to an equation that expresses $\langle q_2 i_c \rangle_0$ as

$$\langle q_2 i_c \rangle_0 = \frac{d_2}{d_1 + d_2} \langle i_c \rangle_0, \quad (16)$$

which is a function of only the index-0 average $\langle i_c \rangle_0$. Since no approximation is made in the derivation process, (16) is precise and equivalent to computing $\langle q_2 i_c \rangle_0$ using discrete convolution with infinite terms, which is not practical to compute directly. Thus replacing (7) by (16) not only decouples the system and improves efficiency but also results in a model with enhanced accuracy. As we will later show in a buck converter simulation example, simulation using the multi-frequency model presented in [8], which approximates $\langle q_2 i_c \rangle_0$ by (7), shows significant errors when the converter operates in DCM. While our proposed model using (16) accurately and efficiently captures converter behaviour in both CCM and DCM.

Now we suggest the second rule of system decoupling which also enhances the accuracy:

Rule 2: For DC-DC converters in any condition, $\langle q_2 i_c \rangle_0 = \frac{d_2}{d_1 + d_2} \langle i_c \rangle_0$. All higher order terms can be removed from the index-0 average calculation without introducing any errors.

Applying rule 2 to $\langle q_2 i_c \rangle_0$ results in the removal of $cs2$ in Fig. 6 as well as changing the current source of $\langle q_2 \rangle_0 \langle i_c \rangle_0$ into $\frac{d_2}{d_1 + d_2} \langle i_c \rangle_0$. Fig. 8 summarizes the decoupled buck converter index-0 average model where all of the components can be evaluated independently of high-order averages. Combining this model with the index-1 average model results in a more efficient and accurate multi-harmonic model.

V. EXPERIMENTAL RESULTS

We test the accuracy and efficiency of our new proposed model by performing simulations of different DC-DC converters and compare the results with two existing averaged models. The first example of the boost converter simulation demonstrates the improved accuracy of our model by considering device non-idealities. The second example of the buck converter simulation shows improved accuracy and efficiency by calculating $\langle q_2 i_c \rangle_0$ using (16). All models and circuits are implemented in Cadence Virtuoso and simulated by Spectre [12]. Our proposed model is described using Verilog-AMS and the converter circuits are described in transistor-level netlists with industry-standard BSIM4 models.

The accuracy of our proposed model is quantified using the following error metric defined with respect to transistor-level simulation:
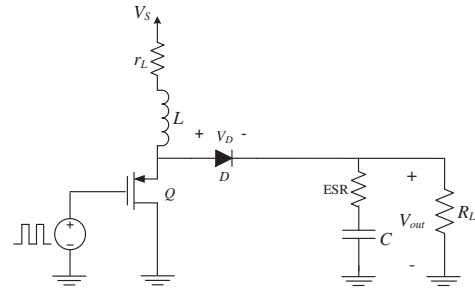
$$\sigma = \frac{\sqrt{\sum_{k=1}^{n} \left(V_{model}(T_s \cdot k) - V(T_s \cdot k)\right)^2}}{\sqrt{\sum_{k=1}^{n} V(T_s \cdot k)^2}} \quad (17)$$

In (17), V is a targeted output voltage obtained by transistor-level simulation while V_{model} is the corresponding output voltage in our proposed model. T_s is the sampling stepsize which is set to one tenth of the switching period of a given converter circuit.

A. Boost Converter Open-loop Simulation

Consider the standard PWM boost converter shown in Fig. 9. A small capacitance value is selected for better demonstration of the ripple. The boost converter operates in CCM with a switching frequency of $f = 50$kHz. For this example, the converter simulation starts with a duty ratio of $d = 0.4$. This ratio is maintained until $t = 0.4$ms at which the duty ratio ramps up to 0.5 and remains at this level for the remainder of the simulation. Fig. 10 shows a comparison of the transistor-level simulation, our proposed model, and the equivalent circuit derived from the in-place circuit averaging with index-0 and index-1 averages considered [10]. The results from the in-place averaging show visible errors in the steady state and the transient state, because it fails to consider the effect of device non-idealities. On the other hand, the output voltage and the inductor current waveforms predicted by our proposed
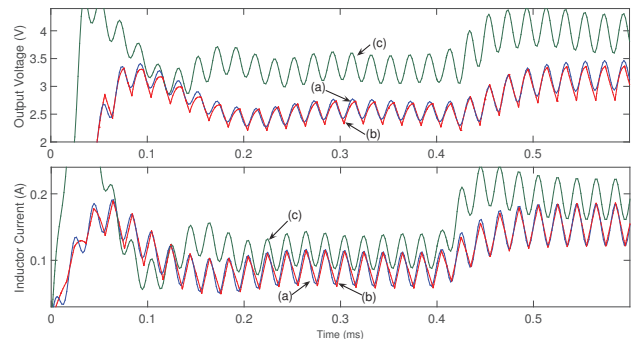

Fig. 10. Boost converter open-loop simulation with varying duty ratio using our proposed model(a), transistor-level circuit(b), and the in-place circuit averaging technique(c).
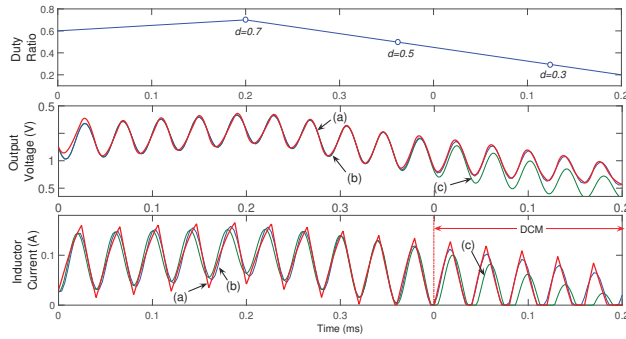
Fig. 11. Buck converter open loop simulation of the transistor-level circuit(a), our proposed model(b), and the modified multi-frequency average model(c).

method match very well with the transistor level simulation. The percentage errors for the output voltage are found to be $\sigma_v = 3.46\%$ using (17). Furthermore, for this example, our proposed model achieved $6X$ runtime speedup with respect to the transistor-level simulation.

B. Buck Converter Open-loop Simulation

Next we test our proposed model on a buck converter operating in CCM and DCM. The stability and robustness of the proposed model is investigated by varying the duty ratio over a wide range. The standard buck converter circuit modeled is shown in Fig. 1(a) with $L = 100\mu H$, $C = 500nF$, $R_L = 10\Omega$ and $f_s = 50kHz$. As shown in Fig. 11(a), the duty ratio is varied in such a way that the converter transitions from CCM to DCM at $t = 0.2ms$.

The simulation results for the output voltage and inductor current of the transistor-level circuit, our proposed model and a modified version of the multi-frequency average model [8] are shown in Fig. 11(b)(c). The multi-frequency average model introduced in [8] does not consider device non-idealities and thus is inaccurate in low-power DC-DC converter simulations. To differ from the previous comparison with in-place averaging, we modified the multi-frequency average model by adding controlled sources that account for device non-idealities including $R_{ds(on)}$, I_{leak} and V_d. As a result, both our model and the multi-frequency model make good predictions of the voltage and current responses in the first $0.2ms$ of simulation when the converter is operating in CCM. However, as the duty ratio continues to drop and the converter enters into DCM, the multi-frequency average model significantly deviates from the true response. The reason for the large errors is that the multi-frequency average model approximates $\langle q_2 i_c \rangle_0$ by (7), which only considers the 0-index and 1-index average and is not accurate when the inductor current i_c is discontinuous. Our proposed model, on the other hand, successfully detects the presence of the DCM and precisely calculates $\langle q_2 i_c \rangle_0$ using (16) and therefore closely tracks the actual circuit response.

In this example, our proposed model replaces the discontinuous inductor current with continuous averaged currents, which results in a $10X$ speedup with respect to the simulation of the transistor-level circuit. The output voltage error in this case is found to be $\sigma_v = 3.97\%$, which once again demonstrates the high accuracy of our proposed model. In comparison, the multi-frequency average model shows an error of $\sigma_v = 18.13\%$. Table I summarizes the speedup and error

of our proposed model with respect to the transistor-level simulations.

TABLE I
ERRORS AND SPEEDUPS OF THE PROPOSED MODEL

	boost converter	buck converter
Transistor-level ckt size	11 nodes	8 nodes
Multi-harmonic ckt size	95 nodes	90 nodes
Error of multi-harmonic ckt	3.46%	3.97%
Speedup over transistor-level ckt	6X	10X

VI. CONCLUSIONS

In this paper we present a multi-harmonic model for PWM DC-DC converters in various topologies. Our proposed model can capture the dc response as well as higher-order harmonics. As a full order model, it retains the inductor current as a state variable and is accurate even when the converter is in the transient state. Our model can seamlessly transition between CCM and DCM during the simulation. Moreover, we suggest two rules for system decoupling in order to achieve better efficiency without compromising accuracy. Our model was tested on two different DC-DC converters and speedups of one order of magnitude were achieved with respect to transistor-level simulations.

VII. ACKNOWLEDGMENTS

REFERENCES

[1] Richard D Middlebrook and Slobodan Ćuk. A general unified approach to modelling switching-converter power stages. *International Journal of Electronics Theoretical and Experimental*, 42(6):521–550, 1977.
[2] Ali Davoudi, Juri Jatskevich, and Tom De Rybel. Numerical state-space average-value modeling of pwm dc-dc converters operating in dcm and ccm. *Power Electronics, IEEE Transactions on*, 21(4):1003–1012, 2006.
[3] Jian Sun, Daniel M Mitchell, Matthew F Greuel, Philip T Krein, and Richard M Bass. Averaged modeling of pwm converters operating in discontinuous conduction mode. *Power Electronics, IEEE Transactions on*, 16(4):482–492, 2001.
[4] Vatche Vorperian. Simplified analysis of PWM converters using model of PWM switch part I: Continuous conduction mode. *IEEE Transactions on Aerospace and Electronic Systems*, 26(3):490–496, May 1990.
[5] Vatché Vorpérian. Simplified analysis of pwm converters using model of pwm switch. ii. discontinuous conduction mode. *Aerospace and Electronic Systems, IEEE Transactions on*, 26(3):497–505, 1990.
[6] Y. Amran, F. Huliehel, and S. Ben-Yaakov. A unified SPICE compatible average model of PWM converters. *IEEE Transactions Electronics*, pages 585–694, 1991.
[7] Seth R Sanders, J Mark Noworolski, Xiaojun Z Liu, and George C Verghese. Generalized averaging method for power conversion circuits. *Power Electronics, IEEE Transactions on*, 6(2):251–259, 1991.
[8] Vahe A Caliskan, OC Verghese, and Aleksandar M Stankovic. Multi-frequency averaging of dc/dc converters. *IEEE Transactions on Power Electronics*, 14(1):124–133, 1999.
[9] DRAGAN Maksimović, ALEKSANDAR M Stanković, V Joseph Thottuvelil, and George C Verghese. Modeling and simulation of power electronic converters. *Proceedings of the IEEE*, 89(6):898–912, 2001.
[10] J Mark Noworolski and Seth R Sanders. Generalized in-plane circuit averaging. In *Applied Power Electronics Conference and Exposition, 1991. APEC'91. Conference Proceedings, 1991., Sixth Annual*, pages 445–451. IEEE, 1991.
[11] Aldrick S Limjoco. Measuring output ripple and switching transients in switching regulators. http://www.analog.com/media/en/technical-documentation/application-notes/AN-1144.pdf.
[12] Cadence Design Systems Inc. Spectre circuit simulator, 2015. http://www.cadence.com/products/cic/spectre_circuit/pages/default.aspx.